Design principle for high-temperature superconductivity in ternary borides at ambient pressure

Zhuangzhuang Qiao,[1] Shuo Cai,[1] Xiaotong Liao,[1] Xiaowei Huang,[1] Liying Zhang,[1] Chongze Wang,[2] J. Cho,[2] Liangliang Liu,[1,3,*] and Yu Jia[1,3,†]

[1]*Key Laboratory for Special Functional Materials of Ministry of Education, School of Nanoscience and Materials Engineering, Henan University, Kaifeng 475004, China*

[2]*Institute for Computational Materials Science, Joint Center for Theoretical Physics (JCTP), School of Physics and Electronics, Henan University, Kaifeng 475004, China*

[3]*Institute of Quantum Materials and Physics, Henan Academy of Sciences, Zhengzhou 450046, China*

(Received 4 June 2025; revised 19 September 2025; accepted 28 October 2025; published 13 November 2025)

The discovery of metal borides with higher transition temperature (T_c) has been receiving continuous attention since the observation of superconductivity in MgB_2 at 39 K. Here we propose a rational design strategy for high-T_c ternary metal borides through the cosubstitution of Mg with two compensating metal elements that possess an effective isovalency of 2. Guided by this principle, we theoretically predict a collection of ternary boride superconductors, including a representative example of $KAlB_4$ that has an isostructure to MgB_2, with T_c up to 67 K at ambient pressure. Our detailed analysis reveals that, compared with MgB_2, due to the Stark effect caused by the difference in valence of two metal ions, the σ bands of B layers get significant splitting and exhibit more flat character, resulting in enhanced electronic occupation; furthermore, the softened in-plane E_{2g} modes produce larger deformation potential and electron-phonon coupling with B σ states, which in turn results in larger superconducting gaps and much higher T_c value in $KAlB_4$. We further propose a feasible synthesis route of $KAlB_4$ to stimulate experimental progress. Our approach paves the way for finding more high-T_c ternary boride superconductors at ambient pressure.

DOI: 10.1103/3cdm-mkdb

I. INTRODUCTION

Ever since Onnes discovered the superconductivity of metal mercury at 4.2 K a century ago [1], it has been one of the most exciting fields of research in condensed matter physics and materials science [2], and tremendous efforts have been devoted to raising the superconducting transition temperature (T_c) in order for potential technological applications [3]. Based on the Bardeen-Cooper-Schrieffer (BCS) theory, light element compounds are believed to be promising candidates for obtaining high-T_c superconductivity since they host high Debye temperature, which is proportional to the T_c [4,5]. Naturally, hydrogen and its hydrides first came into people's attention and a series of high-T_c hydride materials were found under high pressure [6–8]. Representative examples include H_3S, LaH_{10}, CaH_6, and so on, with experimentally measured T_c above 200 K and even approaching room temperature [9–15]. Nevertheless, the pressure required to realize these superconducting hydrides is exceptionally high (>100 GPa) and challenging to achieve, leading to an insurmountable obstacle for any practical application.

Borides, also having high Debye temperature, provide another available option to realize high-temperature superconductivity at ambient pressure. Hexagonal layered MgB_2, discovered by Akimitsu and co-workers in 2001, is a well-known phonon-mediated superconductor with a transition temperature $T_c \approx 39$ K [16], and the in-plane E_{2g} mode was demonstrated to play a central role in the superconducting pair via coupling with B σ states [17,18]. Subsequently, a great deal of effort has been devoted to searching for and designing more boride-derived superconductors in order to obtain higher T_c by substituting Mg atoms or partially doping other elements experimentally and theoretically [19–32]. Regrettably, the implementation of this approach in MgB_2 systems leads to degradation and even elimination of superconductivity, or compromised structural integrity demanding high-pressure environments for phase stabilization. For instance, Rosner *et al.* suggested that the layered semiconductor LiBC, isovalent to MgB_2, could transform into metal and host superconductivity at ≈100 K by introducing Li vacancies; however, a subsequent experiment found that Li deficiency would induce dramatic structural distortions of B-C layers and destroy the superconductivity [33,34]. Pei *et al.* recently discovered that α-MoB_2, having the same structure as MgB_2, exhibited the second-highest T_c of 32 K above 60 GPa [35,36]. Additionally, a series of MgB_2-like layered borocarbide films such as CaB_2C_2, KB_2C_2, and LaB_2C_2 were predicted to exhibit high T_c of ≈80 K at ambient pressure due to their strong metallic σ states of B-C layers [27,37,38], but, because B and C atoms have very similar masses, it is extremely difficult to precisely control alternating B-C bonding to form a perfect honeycomb lattice during thin-film growth; we are not aware of subsequent experimental progress on these predictions.

In doing so, surrounding MgB_2, we propose a rational design strategy for high-T_c ternary metal borides through the cosubstitution of Mg with two compensating metal elements

*Contact author: liull@henu.edu.cn
†Contact author: jiayu@henu.edu.cn

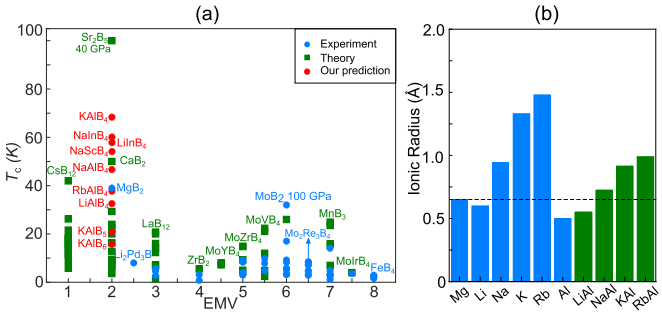

FIG. 1. (a) The superconducting transition temperature as a function of the effective metal valency. The existing systems predicted by theory and identified by experiment in the previous literature are marked by green squares and blue dots, respectively, while the newly predicted systems are denoted by red dots [see the data in Table S1 of the Supplemental Material (SM) [44]]. The ionic radii of metals are shown in (b), and for the dual alloy, the average ionic radius of two metal atoms is used.

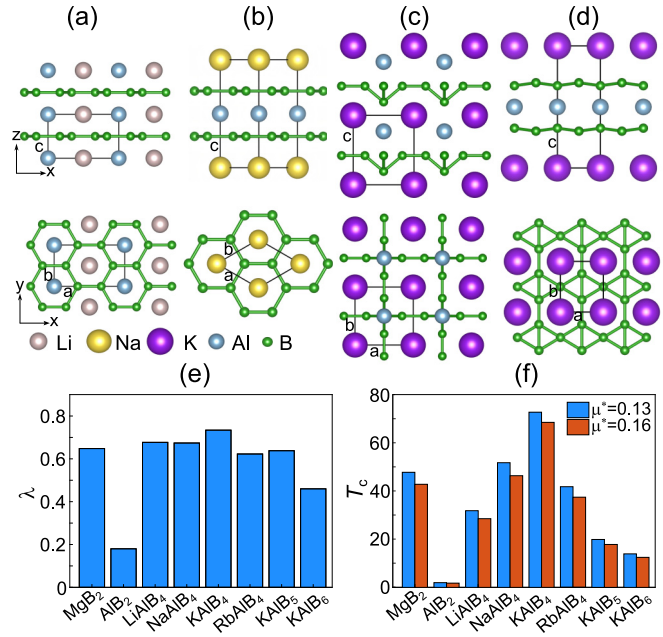

FIG. 2. The predicted new boride structures (a) *Pmmm*$LiAlB_4$, (b) *P6/mmm*$NaAlB_4$, (c) *P4mm*$KAlB_5$, and (d) *Pmmm*$KAlB_6$. $KAlB_4$ and $RbAlB_4$ also adopt the same space group as $NaAlB_4$. (e) The calculated total EPC constant λ of ternary borides, in comparison with those of MgB_2 and AlB_2. (f) The estimated T_c values of metal borides by using the anisotropic Migdal-Eliashberg equations.

in terms of valence electrons and ionic radius, and here dual metal elements A (A = Li, Na, K, and Rb) and Al are chosen as model systems. On the one hand, two compensatory metal atoms possess effective metal valency of 2, which is beneficial to stabilize the B atomic layer and metallize its σ states simultaneously. In MgB_2, B atoms form a graphitelike honeycomb layer, but with only three valence electrons the layer is not stable, and intercalated Mg stabilizes it by transferring two electrons to the B layer. Meanwhile, Mg^{2+} has a stronger electrostatic attraction with the π electrons of the B layer, which lowers the π bands and results in a $\sigma \rightarrow \pi$ charge transfer that induces the hole doping of σ bands, and thus B σ states get metallization associated with emergent large occupation at the Fermi level (E_F) [17]. Deviation from two valence electrons disrupts this balance: fewer electrons (e.g., alkali-metal borides [39,40]) prevent the formation of the honeycomb structure, while excess doping (e.g., AlB_2 or transition-metal borides such as ScB_2 and ZrB_2) shifts σ states below the E_F [22,41–43]. Therefore, as the effective metal valency (EMV) increases or decreases from 2, the T_c is distinctly lowered, as shown in Fig. 1(a). On the other hand, by adjusting the ionic radius of alloy atoms [from smaller to larger than Mg^{2+} [see Fig. 1(b)]] through the variation in alkali metal, it would open up possibilities to effectively modulate the B-B σ-bond length and strength to realize the optimal metallization of σ states, in order to obtain stronger electron-phonon coupling (EPC) and higher T_c superconductivity at ambient pressure.

Based on this motivation, we performed a comprehensive first-principles calculation [45] and structure searches for the ternary metal borides A-Al-B_y (y = 3–9) at ambient pressure via the swarm-intelligence-based calypso code [46,47], and predicted a collection of new boride superconductors. Among them, *P6/mmm*$KAlB_4$, which is isostructural to MgB_2, exhibits higher T_c of 67 K. Our detailed analysis demonstrates that the Stark effect, caused by the difference in valence of K and Al ions, drives the σ bands of B layers to get significant splitting energetically associated with the emergence of more flat dispersion, enhancing electronic occupation of σ states at E_F; furthermore, the softened in-plane E_{2g} modes strongly couple with Fermi surface (FS) σ states, producing larger deformation potential and EPC strength, which induces larger superconducting gaps and higher T_c in $KAlB_4$ than MgB_2. The calculated results indicate that the compensatory cosubstitution strategy provides a feasible way to design higher-T_c ternary metal boride superconductors.

II. RESULTS

The main results of convex hull diagrams for A-Al-B_y are shown in Figs. S1 and S2 of the Supplemental Material (SM) [44], and considering the non-negligible quantum effects associated with the relatively light B atom, the contributions of the zero-point energies were included in all our calculations of the formation enthalpies for the ternary borides. From the structural searching, four classes of stable structures are obtained at ambient pressure, including *Pmmm*$LiAlB_4$, *P6/mmm*$NaAlB_4$/$KAlB_4$/$RbAlB_4$, *P4mm*$KAlB_5$, and *Pmmm*$KAlB_6$. The detailed structural information is shown in Figs. 2(a)–2(d) and listed in Table S2 of the SM [44]. *Pmmm*$LiAlB_4$, having a layered structure similar to that of AlB_2, can be obtained by substituting half of the Al atoms in $\sqrt{3} \times 1 \times 1$ AlB_2 with Li atoms, and Li and Al atoms are spaced apart in the honeycomb center of the B layer. Three *P6/mmm* phases $NaAlB_4$, $KAlB_4$, and $RbAlB_4$ also originate from AlB_2, and they adapt the double cells of AlB_2 ($1 \times 1 \times 2$ primitive cell) along the c axis with one Al atom layer replaced by Na, K, or Rb atoms, respectively. Here, due to the radius difference of three alkali-metal ions, the formed borides have different lattice constants, interlayer

space, and B-B bond length and strength, which could greatly influence the σ state distribution, phonon frequency, and EPC strength, as discussed below. In addition, we find another two novel ternary borides that are dynamically stable. Specially, in $P4mm$KAlB$_5$, B atoms form a one-dimensional chainlike structure, intertwined in mutually orthogonal directions, and this structure provides a platform to study one-dimensional superconductivity. For the $Pmmm$KAlB$_6$, B atoms also adopt layered structures, formed by triangles and hexagonal rings. These searching results demonstrate that the compensatory cosubstitution provides an effective route to design more metal borides.

Having investigated the stability and structural information of these ternary borides, we focus on their superconducting properties. From the Eliashberg equations [48,49], the total EPC strength λ and the values of T_c with typical Coulomb pseudopotential parameters from 0.13 to 0.16 [36,50,51] were calculated, and the corresponding results of MgB_2 are also listed as comparison, as shown in Figs. 2(e) and 2(f). As shown in Fig. 2(e), $KAlB_4$ hosts the largest EPC constant λ of 0.75 among the studied compounds, which is larger than $\lambda = 0.64$ of MgB_2. Correspondingly, Fig. 2(f) shows that the $KAlB_4$ obtains the highest T_c of 67–73 K by using the anisotropic Migdal-Eliashberg equations, significantly higher than the calculated value of MgB_2 ($T_c = 44$–47 K). Here, it needs to be noted that anisotropic Migdal-Eliashberg equations would slightly overestimate the T_c, higher than the experimental value measured at 39 K in MgB_2, and this phenomenon is also found in other boride and hydride superconductors [35,36,52–54]. Likewise, the λ and T_c of $NaAlB_4$ are estimated to be 0.67 and 47–52 K, respectively, slightly larger than those of MgB_2. In addition, the T_c of $LiAlB_4$, $RbAlB_4$, $KAlB_5$, and $KAlB_6$ are predicted to be 28, 38, 20, and 14 K with $\mu^* = 0.16$, respectively. We note that $NaAlB_4$, $KAlB_4$, and $RbAlB_4$ have similar structures to MgB_2, while $KAlB_4$ obtains the highest T_c, which indicates that dual metals K and Al make the B layers realize optimal metallization of σ states, and thus effectively couple to the mode E_{2g}, as discussed below.

To reveal how such compensatory cosubstitution behaves synergistically to enhance the EPC and obtain a higher T_c in $KAlB_4$, we here make comparative discussions of MgB_2, and the calculated results of other ternary borides are shown in Figs. S3–S5 of the SM [44]. Since the λ and T_c are closely related to the FS states, phonon frequencies, and their coupling strength, we first examine the electronic properties of $KAlB_4$ by modeling the band structures and density of states (DOS) as shown in Figs. 3(a) and 3(b). The projected band structure shows that dual metals K and Al effectively tune the σ bands to be across the E_F, forming four cylindrical FS sheets surrounding the Γ point (see Fig. S6 of the SM [44]). Meanwhile, it is noteworthy that, due to valence imbalance between K ($\sim+1$) and Al ($\sim+3$) ions (see Fig. S7 in the SM [44]), the B layers on both sides experience unequal external electric field, e.g., inducing a Stark effect. This leads to a splitting of the σ bands into two regimes of σ_1 and σ_2, with the σ_1 regime shifting closer to the E_F. Compared to the MgB_2 (see band structure in Fig. S8 of the SM [44]), these σ_1 and σ_2 bands exhibit stronger two-dimensional characteristics, and their band dispersions along path Γ-A are much flatter.

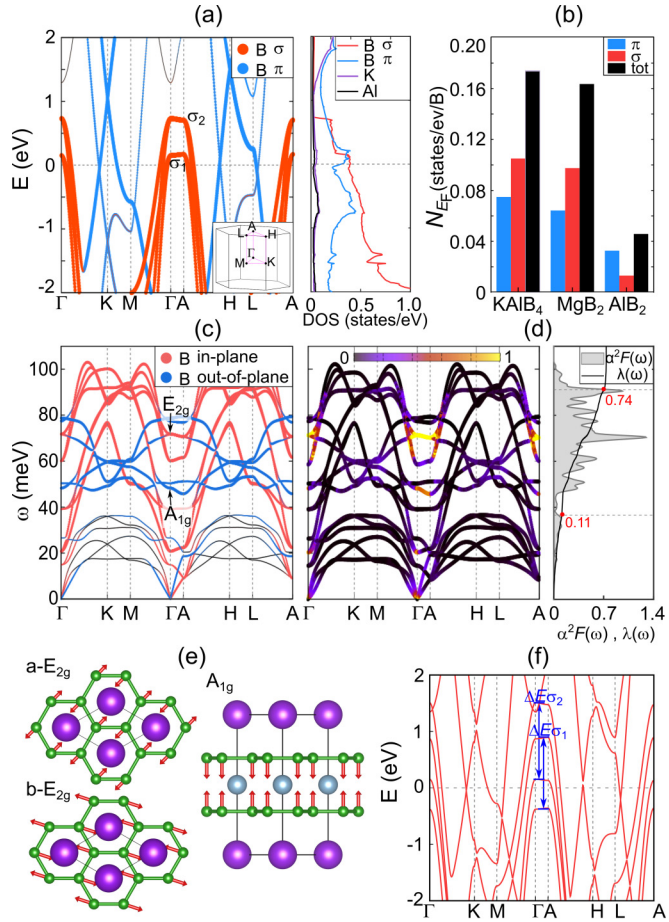

FIG. 3. (a) Calculated band structure and partial DOS for $KAlB_4$. (b) Electronic states at E_F (N_{E_F}) per B atom of $KAlB_4$, in comparison with those of MgB_2 and AlB_2. (c) Phonon spectrum projected on B atomic in-plane (x, y) and out-of-plane (z) vibrations. (d) Phonon spectrum with projection of EPC parameter $\lambda_{q\nu}$ using the color scale in the range [0,1], and the isotropic Eliashberg spectral function $\alpha^2F(\omega)$ with integrated EPC constant $\lambda(\omega)$. (e) Two kinds of atomic displacements of the E_{2g} mode, marked by a-E_{2g} and b-E_{2g}, and atomic displacement of the A_{1g} mode. The arrows indicate the vibrational directions of atoms. (f) Band structure with the atomic displacement of the a-E_{2g}.

Therefore the obtained electronic occupation at E_F per B atom (N_{E_F}) of $KAlB_4$ gets enhanced, and the N_{E_F} value is larger than that of MgB_2. Also the N_{E_F} is much larger than that of AlB_2 since its σ bands are mainly located ≈ 1.0 eV below E_F at the Γ pont (see Fig. S8 of the SM [44]). In short, the compensatory cosubstitution of K and Al effectively increases the contribution of the electronic state of the B sublattice.

Next, we move on to examine the phonon vibration and EPC within density functional perturbation theory (DFPT) [55]. Figure 3(c) presents the phonon spectrum with projected atom vibration. It is seen that the optical branches mainly arise from the in-plane and out-of-plane vibrations of B atoms, exhibiting a large band dispersion, and these B-atom vibrations produce very strong EPC, nearly accounting for $\approx$85% of the total EPC constant $\lambda = 0.75$ [see Fig. 3(d)]. Specifically, at the Γ point, in-plane stretching modes E_{2g} suffer from the softeness in frequency, and give rise to a

sharp peak in the spectral function $\alpha^2F(\omega)$ at ≈72 meV, obtaining the largest EPC parameter $\lambda_{q\nu}$ [see Fig. 3(d)]. Figure 3(e) shows the two kinds of atomic displacements in the modes E_{2g}. In order to further quantitatively evaluate the coupling strength of the modes E_{2g}, deformation potentials were calculated based on the equation $D \equiv \Delta E_k/\Delta q$ [17,56], and the underlying concept is that a phonon with mode amplitude q that is strongly coupled to FS states will produce a large energetic shift in k (ΔE_k) for states near the E_F. Figure 3(f) shows the calculated band structures with the atomic displacement a-E_{2g}, and the result of atomic displacement b-E_{2g} is shown in Fig. S9 of the SM [44]. It is seen in Fig. 3(f) that the phonon strongly splits the σ_1 and σ_2 bands along the Γ-A line with the maximum gap opening reaching 1.25 and 1.36 eV, and the obtained deformation potentials D_{σ_1} and D_{σ_2} are 15.3 and 16.6 eV/Å, respectively. It is noted that these two values are larger than the previously reported $D_\sigma = 13$ eV/Å of MgB_2 [17], exhibiting a stronger coupling, which highlights the key role of E_{2g} modes in producing strong EPC in $KAlB_4$. Additionally, we note that another softened phonon mode A_{1g}, out-of-plane vibrations of B atoms, also obtains the large parameter $\lambda_{q\nu}$ by compressing π bonds, contributing to a significant peak in the $\alpha^2F(\omega)$. The above phonon and EPC analysis clearly demonstrates that B in-plane and out-of-plane phonon modes contribute to very strong EPC, obtaining a larger λ value than MgB_2, implying these two types of phonon-modulated electron pairing would produce larger superconducting gaps and higher T_c in $KAlB_4$.

Furthermore, considering the anisotropic distribution of electronic states on the FS in $KAlB_4$, the anisotropic Migdal-Eliashberg equations were used to reveal the k-resolved EPC parameter λ_{nk} and superconducting gap Δ_{nk} for the electronic states (n, k). The n represents the band index, and all available electron-phonon scattering processes connecting k and other k points on the FS sheets are included, as employed in MgB_2 superconducting analysis [18]. The distribution of the λ_{nk} and Δ_{nk} are displayed in Figs. 4(a) and 4(b), respectively. It is shown that the λ_{nk} value on the FS exhibits significant anisotropy, and there are two regimes λ_σ and λ_π, that is, the larger regime λ_σ in the range 1.1–1.8 is contributed by B σ_1 and σ_2 states [see orbital distribution in Fig. 4(c)], and the smaller one λ_π in the range 0.3–0.7 is by B π states. It represents that B σ states give rise to the large λ_{nk}, which is consistent with the calculated results that modes E_{2g} could produce the largest EPC parameter $\lambda_{q\nu}$ by stretching B-B σ bonds.

Naturally, two anisotropic distributions can give rise to two well-separated superconducting gaps, showing the feature of two-gap superconductivity [see Figs. 4(d) and 4(e)], as in the case of MgB_2. For the k-resolved superconducting gap Δ_{nk}, it is noted that the Δ_{nk} and λ_{nk} are correlated with each other; i.e., the larger the λ_{nk} strength, the higher the Δ_{nk} value. At 5 K, the larger gap Δ_σ (the smaller one Δ_π) lies in the range 8–12 meV (1.5–5 meV), and the separation of energy between Δ_σ and Δ_π is ≈3.0 meV. Compared to MgB_2, it is noteworthy that the maximum value of Δ_σ is 12 meV, larger than 9 meV in MgB_2, indicating a larger Cooper pair binding energy for $KAlB_4$. Figure 4(d) shows the calculated normalized quasiparticle DOS in the superconducting state of $KAlB_4$, according to $\frac{N_S(\omega)}{N_F} = \mathrm{Re}[\frac{\omega}{\sqrt{\omega^2-\Delta^2(\omega)}}]$, which can be

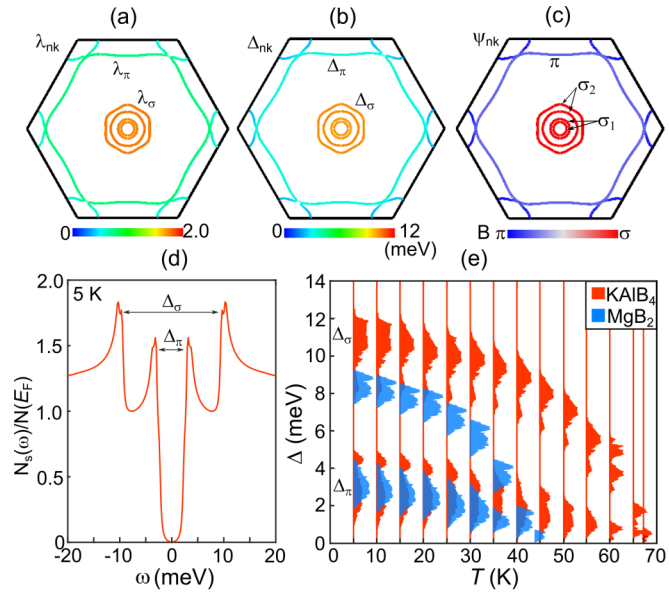

FIG. 4. Calculated k-resolved (a) EPC parameter λ_{nk}, (b) superconducting gap Δ_{nk} at 5 K, and (c) two-dimensional FS sheets, colored by the B orbital character $(\sigma - \pi)/(\sigma + \pi)$. (d) The normalized quasiparticle DOS at 5 K. (e) Energy distribution of the anisotropic superconducting gap Δ versus T for $KAlB_4$ and MgB_2.

used to compare with the experimental tunneling conductance directly [52]. It is seen that there are two pairs of peaks, corresponding to two superconducting gaps. As the temperature T increases, two gaps Δ_σ and Δ_π gradually decrease, reaching zero at approximately 67 K with $\mu^* = 0.16$, obtaining a larger T_c than 44 K of MgB_2 [see Fig. 4(e)]. For comparison, we note that Sr_2B_5, with a unique covalent sp^3-hybridized B framework, exhibits a higher T_c of above 100 K, while it needs to remain structurally stable above 40 GPa, limiting further experimental synthesis and measurement [70]. A high-throughput approach was employed to screen a large number of stable ternary metal borides, and Li_3ZrB_8 was predicted to exhibit 38 K superconductivity [57]. Recently, a new superatomic structure CsB_{12}, in which B_{12} icosahedral clusters assemble into a simple cubic lattice, was predicted with T_c reaching 42 K [58], compared to MgB_2. Overall, to our knowledge, $KAlB_4$ is the highest-T_c metal boride superconductor at ambient pressure, urgently requiring future experimental verification.

Finally, we would like to discuss how to reasonably synthesize this boride $KAlB_4$ in experiment, since the previous research has predicted lots of high-T_c boride superconductors but fewer compounds were synthesized. Although the calculated formation energy above the convex hull (E_d) demonstrates $KAlB_4$ is a metastable structure according to the full ternary convex hull diagram (see Fig. S2 of the SM [44]), it becomes thermodynamically stable when the references are restricted to the experimentally synthesized compounds KB, KB_6, and AlB_2. The feasible route is $4KB + KB_6 + 5AlB_2 \rightarrow 5KAlB_4$, and the corresponding reaction is exothermic, as shown in Fig. S10 of the SM [44]. Molecular dynamics calculations also predict that the B honeycomb framework in $KAlB_4$ retains its structural integrity even at

elevated temperatures (see Fig. S11 of the SM [44]). Therefore, the vapor deposition method [59–61] may be used to synthesize this $KAlB_4$ at high temperature.

III. SUMMARY

In conclusion, we have proposed a rational design strategy for high-T_c ternary metal borides through two compensating metal elements that possess an effective isovalency of 2, and we predicted a series of new strong EPC superconducting boride compounds. The representative example of the two-gap superconductor $KAlB_4$ exhibits larger EPC strength and higher T_c than MgB_2, which originates from the fact that dual alloy effectively enhances electronic states of the B layer and the coupling strength of the E_{2g} mode. We also propose a reliable synthesis route for $KAlB_4$ by using the known boride precursors, which will stimulate further experimental synthesis and identification. In addition, we found $LiInB_4$, $NaInB_4$, and $NaScB_4$, having the same structures as $KAlB_4$, are dynamically stable, and also exhibit high-temperature superconductivity of $T_c = 53$–60 K, since dual metal atoms have an EMV of 2 and effectively metallize the B σ states (see Figs. S12 and S13 of the SM [44]). Our results demonstrate that the strategy of two compensating metal elements with effective isovalency of 2 indeed provides a feasible route to design more high-T_c boride superconductors, and we can anticipate that this principle is likely more universal and true for binary, ternary, and even potentially higher multiple-component metal borides.

ACKNOWLEDGMENTS

We acknowledge support from Natural Science Foundation of Henan Province (Grants No. 242300421162 and No. 242300421213), the National Natural Science Foundation of China (Grants No. 12104129 and No. 12074099), and the Innovation Program for Quantum Science and Technology (Grant No. 2021ZD0302800).

DATA AVAILABILITY

The data supporting this study's findings are available within the article.

[1] H. K. Onnes, The resistance of pure mercury at helium temperatures, Commun. Phys. Lab. Univ. Leiden **120b** (1911), reprinted in Proc. K. Ned. Akad. Wet. **13**, 1274 (1911).
[2] I. I. Mazin, Extraordinarily conventional, Nature (London) **525**, 40 (2015).
[3] J. A. Flores-Livas, L. Boeri, A. Sanna, G. Profeta, R. Arita, and M. Eremets, A perspective on conventional high-temperature superconductors at high pressure: Methods and materials, Phys. Rep. **856**, 1 (2020).
[4] J. Bardeen, L. N. Cooper, and J. R. Schrieffer, Microscopic theory of superconductivity, Phys. Rev. **106**, 162 (1957).
[5] N. W. Ashcroft, Metallic hydrogen: A high-temperature superconductor? Phys. Rev. Lett. **21**, 1748 (1968).
[6] J. M. McMahon and D. M. Ceperley, High-temperature superconductivity in atomic metallic hydrogen, Phys. Rev. B **84**, 144515 (2011).
[7] J. M. McMahon, M. A. Morales, C. Pierleoni, and D. M. Ceperley, The properties of hydrogen and helium under extreme conditions, Rev. Mod. Phys. **84**, 1607 (2012).
[8] N. W. Ashcroft, Hydrogen dominant metallic alloys: High temperature superconductors? Phys. Rev. Lett. **92**, 187002 (2004).
[9] H. Wang, J. S. Tse, K. Tanaka, T. Iitaka, and Y. Ma, Superconductive sodalite-like clathrate calcium hydride at high pressures, Proc. Natl. Acad. Sci. USA **109**, 6463 (2012).
[10] F. Peng, Y. Sun, C. J. Pickard, R. J. Needs, Q. Wu, and Y. Ma, Hydrogen clathrate structures in rare earth hydrides at high pressures: Possible route to room-temperature superconductivity, Phys. Rev. Lett. **119**, 107001 (2017).
[11] H. Liu, I. I. Naumov, R. Hoffmann, N. W. Ashcroft, and R. J. Hemley, Potential high-T_c superconducting lanthanum and yttrium hydrides at high pressure, Proc. Natl. Acad. Sci. USA **114**, 6990 (2017).
[12] A. P. Drozdov, M. I. Eremets, I. A. Troyan, V. Ksenofontov, and S. I. Shylin, Conventional superconductivity at 203 Kelvin at high pressures in the sulfur hydride system, Nature (London) **525**, 73 (2015).
[13] A. P. Drozdov, P. P. Kong, V. S. Minkov, S. P. Besedin, M. A. Kuzovnikov, S. Mozaffari, L. Balicas, F. F. Balakirev, D. E. Graf, V. B. Prakapenka *et al.*, Superconductivity at 250 K in lanthanum hydride under high pressures, Nature (London) **569**, 528 (2019).
[14] M. Somayazulu, M. Ahart, A. K. Mishra, Z. M. Geballe, M. Baldini, Y. Meng, V. V. Struzhkin, and R. J. Hemley, Evidence for superconductivity above 260 K in lanthanum superhydride at megabar pressures, Phys. Rev. Lett. **122**, 027001 (2019).
[15] L. Ma, K. Wang, Y. Xie, X. Yang, Y. Y. Wang, M. Zhou, H. Y. Liu, X. H. Yu, Y. S. Zhao, H. B. Wang, G. T. Liu, and Y. M. Ma, High-temperature superconducting phase in clathrate calcium hydride CaH_6 up to 215 K at a pressure of 172 GPa, Phys. Rev. Lett. **128**, 167001 (2022).
[16] J. Nagamatsu, N. Nakagawa, T. Muranaka, Y. Zenitani, and J. Akimitsu, Superconductivity at 39 K in magnesium diboride, Nature (London) **410**, 63 (2001).
[17] J. M. An and W. E. Pickett, Superconductivity of MgB_2: Covalent bonds driven metallic, Phys. Rev. Lett. **86**, 4366 (2001).
[18] H. J. Choi, D. Roundy, H. Sun, M. L. Cohen, and S. G. Louie, The origin of the anomalous superconducting properties of MgB_2, Nature (London) **418**, 758 (2002).
[19] H. Rosner, W. E. Pickett, S. L. Drechsler, A. Handstein, G. Behr, G. Fuchs, K. Nenkov, K. H. Muller, and H. Eschrig, Electronic structure and weak electron-phonon coupling in TaB_2, Phys. Rev. B **64**, 144516 (2001).
[20] J. S. Slusky, N. Rogado, K. A. Regan, M. A. Hayward, P. Khalifah, T. He, K. Inumaru, S. M. Loureiro, M. K. Haas, H. W. Zandbergen, and R. J. Cava, Loss of superconductivity with the addition of Al to MgB_2 and a structural transition in $Mg_{1-x}Al_xB_2$, Nature (London) **410**, 343 (2001).
[21] N. I. Medvedeva, A. L. Ivanovskii, J. E. Medvedeva, and A. J. Freeman, Electronic structure of superconducting MgB_2 and

related binary and ternary borides, Phys. Rev. B **64**, 020502(R) (2001).
[22] N. Barbero, T. Shiroka, B. Delley, T. Grant, A. J. S. Machado, Z. Fisk, H.-R. Ott, and J. Mesot, Doping-induced superconductivity of ZrB_2 and HfB_2, Phys. Rev. B **95**, 094505 (2017).
[23] C. Buzea and T. Yamashita, Review of the superconducting properties of MgB_2, Supercond. Sci. Technol. **14**, R115 (2001).
[24] L. Zhu, G. M. Borstad, H. Y. Liu, P. A. Guńka, M. Guerette, J.-A. Dolyniuk, Y. Meng, E. Greenberg, V. B. Prakapenka, B. L. Chaloux *et al.*, Carbon-boron clathrates as a new class of sp^3-bonded framework materials, Sci. Adv. **6**, eaay8361 (2020).
[25] L. Zhu, H. Liu, M. Somayazulu, Y. Meng, P. A. Guńka, T. B. Shiell, C. Kenney-Benson, S. Chariton, V. B. Prakapenka, H. Yoon, J. A. Horn, J. Paglione, R. Hoffmann, R. E. Cohen, and T. A. Strobel, Superconductivity in SrB_3C_3 clathrate, Phys. Rev. Res. **5**, 013012 (2023).
[26] N. Geng, K. P. Hilleke, L. Zhu, X. Wang, T. A. Strobel, and E. Zurek, Conventional high-temperature superconductivity in metallic, covalently bonded, binary-guest C-B clathrates, J. Am. Chem. Soc. **145**, 1696 (2023).
[27] Y. Zhang, J. Chen, J. Hao, M. Xu, and Y. Li, Conventional high-temperature superconductivity in σ-band driven metallized two-dimensional metal borocarbides, Phys. Rev. B **110**, 064513 (2024).
[28] J. Li, J. Yue, S. Guo, A. Zhang, L. Zhu, H. Song, Z. Liu, Y. Liu, and T. Cui, High-temperature superconductivity of boron-carbon clathrates at ambient pressure, Phys. Rev. B **109**, 144509 (2024).
[29] J. Wei, T. Zhong, J. Sun, H. Liu, L. Zhu, and S. Zhang, Electride states and superconductivity in unconventional stoichiometric aluminum borides, Phys. Rev. B **111**, 184508 (2025).
[30] W. Hayami, X. Rocquefelte, and J.-F. Halet, Possible superconductivity for layered metal boride carbide compounds MB_2C_2 (M = alkali, alkaline-earth, or rare-earth metals), Inorg. Chem. **63**, 20975 (2024).
[31] X. R. Jia, A. L. Liu, X. Zhong, and H. Y. Liu, Research progress in multi-boron-carbon-based high-temperature superconductors under high pressures, Chin. J. High Pressure Phys. **39**, 090201 (2025).
[32] P. Zhang, X. Li, X. Yang, H. Wang, Y. Yao, and H. Liu, Path to high-T_c superconductivity via Rb substitution of guest metal atoms in the SrB_3C_3 clathrate, Phys. Rev. B **105**, 094503 (2022).
[33] H. Rosner, A. Kitaigorodsky, and W. E. Pickett, Prediction of high T_c superconductivity in hole-doped LiBC, Phys. Rev. Lett. **88**, 127001 (2002).
[34] A. M. Fogg, J. Meldrum, G. R. Darling, J. B. Claridge, and M. J. Rosseinsky, Chemical control of electronic structure and superconductivity in layered borides and borocarbides: Understanding the absence of superconductivity in Li_xBC, J. Am. Chem. Soc. **128**, 10043 (2006).
[35] C. Y. Pei, J. F. Zhang, Q. Wang, Y. Zhao, L. L. Gao, C. S. Gong, S. J. Tian, R. T. Luo, M. T. Li, W. G. Yang, Z. Y. Lu, H. C. Lei, K. Liu, and Y. P. Qi, Pressure-induced superconductivity at 32 K in MoB_2, Nat. Sci. Rev. **10**, nwad034 (2023).
[36] X. H. Liu, X. W. Huang, P. Song, C. Z. Wang, L. Y. Zhang, P. Lv, L. L. Liu, W. F. Zhang, J. H. Cho, and Y. Jia, Strong electron-phonon coupling superconductivity in compressed α-MoB_2 induced by double van Hove singularities, Phys. Rev. B **106**, 064507 (2022).
[37] L. Liu, X. Liu, P. Song, L. Zhang, X. Huang, W. Zhang, Z. Zhang, and Y. Jia, Surface superconductivity with high transition temperatures in layered $Ca_nB_{n+1}C_{n+1}$, Nano Lett. **23**, 1924 (2023).
[38] H. D. Liu, X. P. Fu, Z. G. Fu, H. Y. Lu, and P. Zhang, High-T_c and three-gap two-dimensional superconductors with electronic and phononic topology: KB_2C_2, Phys. Rev. B **111**, 184502 (2025).
[39] A. N. Kolmogorov and S. Curtarolo, Theoretical study of metal borides stability, Phys. Rev. B **74**, 224507 (2006).
[40] H. Rosner and W. E. Pickett, Theoretical investigation of stoichiometric lithium monoboride, Phys. Rev. B **67**, 054104 (2003).
[41] K.-P. Bohnen, R. Heid, and B. Renker, Phonon dispersion and electron-phonon coupling in MgB_2 and AlB_2, Phys. Rev. Lett. **86**, 5771 (2001).
[42] M. Dahlqvist, U. Jansson, and J. Rosen, Influence of boron vacancies on phase stability, bonding, structure of MB_2, (M = Ti, Zr, Hf, V, Nb, Ta, Cr, and Mo, W) with AlB_2 type structure, J. Phys.: Condens. Matter **27**, 435702 (2015).
[43] S. M. Sichkar and V. N. Antonov, Electronic structure, phonon spectra and electron-phonon interaction in ScB_2, Low Temp. Phys. **39**, 595 (2013).
[44] See Supplemental Material at http://link.aps.org/supplemental/10.1103/3cdm-mkdb for structural information, superconducting transition temperature, convex hull, phonon spectra, the total EPC constant, electronic density of states, band structures, Fermi surface, and superconducting gaps, which includes Refs. [16,23,35,43,57,58,62–108].
[45] Our density functional theory (DFT) calculations were performed using the Vienna Ab initio Simulation Package with the projector augmented-wave method [109–111]. The generalized-gradient approximation functional of Perdew, Burke, and Ernzerhof (PBE) [112] was used to deal with the exchange-correlation energy, and a plane-wave basis was taken with a kinetic-energy cutoff of 600 eV. The k-space integration was performed with a $15 \times 15 \times 15k$-point grid for the structure optimization, allowing all atoms to relax along the calculated forces until all the residual force components were less than 0.005 eV/Å. The lattice dynamics and electron-phonon coupling (EPC) calculations for A-Al-B_y were carried out using the quantum espresso (QE) package [113] V, with the optimized norm-conserving anderbilt (ONCV) pseudopotentials [114]. The plane-wave cutoff and the energy cutoff for charge density were set as 70 and 280 Ry, respectively. The convergence criteria of energy and force were set to 10^{-12} Ry and 10^{-12} RyM/bohr, respectively, and Varzari-anderbilt smearing of 0.02 Ry was used. For the phonon calculations, a $5 \times 5 \times 3q$ M-point grid was employed. The solutions of the fully anisotropic Eigdal-liashberg equations with interpolated k-point grid of $48 \times 48 \times 48$ and a q-point grid of $24 \times 24 \times 24$ were employed to calculate the EPC parameter and superconducting gaps, as implemented in the electron-phonon Wannier (EPW) code [115,116]. Electrons within ±500 meV from the Fermi energy are taken into the EPC process. Then, the corresponding EPC and superconducting properties of each structure were obtained.

[46] Y. Wang, J. Lv, L. Zhu, and Y. Ma, CALYPSO: A method for crystal structure prediction, Comput. Phys. Commun. **183**, 2063 (2012).

[47] Y. Wang, J. Lv, L. Zhu, and Y. Ma, Crystal structure prediction via particle-swarm optimization, Phys. Rev. B **82**, 094116 (2010).

[48] H. J. Choi, M. L. Cohen, and S. G. Louie, Anisotropic Eliashberg theory of MgB_2: T_c, isotope effects, superconducting energy gaps, quasiparticles, and specific heat, Physica C **385**, 66 (2003).

[49] A. Sanna, J. A. Flores-Livas, A. Davydov, G. Profeta, K. Dewhurst, S. Sharma, and E. K. U. Gross, *Ab initio* Eliashberg theory: Making genuine predictions of superconducting features, J. Phys. Soc. Jpn. **87**, 041012 (2018).

[50] P. P. Singh, Theoretical study of electron-phonon interaction in ZrB_2 and TaB_2, Phys. Rev. B **69**, 094519 (2004).

[51] J. Bekaert, M. Petrov, A. Aperis, P. M. Oppeneer, and M. V. Milošević, Hydrogen-induced high-temperature superconductivity in two-dimensional materials: The example of hydrogenated monolayer MgB_2, Phys. Rev. Lett. **123**, 077001 (2019).

[52] E. R. Margine and F. Giustino, Anisotropic Migdal-Eliashberg theory using Wannier functions, Phys. Rev. B **87**, 024505 (2013).

[53] C. Heil, S. Di Cataldo, G. B. Bachelet, and L. Boeri, Superconductivity in sodalite-like yttrium hydride clathrates, Phys. Rev. B **99**, 220502 (R) (2019).

[54] P. Kong, V. S. Minkov, M. A. Kuzovnikov, A. P. Drozdov, S. P. Besedin, S. Mozaffari, L. Balicas, F. F. Balakirev, V. B. Prakapenka, S. Chariton *et al.*, Superconductivity up to 243 K in the yttrium-hydrogen system under high pressure, Nat. Commun. **12**, 5075 (2021).

[55] S. Baroni, S. de Gironcoli, A. Dal Corso, and P. Giannozzi, Phonons and related crystal properties from density-functional perturbation theory, Rev. Mod. Phys. **73**, 515 (2001).

[56] F. S. Khan and P. B. Allen, Deformation potentials and electron-phonon scattering: Two new theorems, Phys. Rev. B **29**, 3341 (1984).

[57] R. Wang, Y. Sun, F. Zhang, F. Zheng, Y. Fang, S. Wu, H. Dong, C.-Z. Wang, V. Antropov, and K.-M. Ho, High-throughput screening of strong electron-phonon couplings in ternary metal diborides, Inorg. Chem. **61**, 18154 (2022).

[58] S. D. Cataldo, A. Sanna, and L. Boeri, Ambient-pressure superconductivity from boron icosahedral superatoms, arXiv:2508.17422.

[59] L. Z. Sun, G. W. Yuan, L. B. Gao, J. U. Yang, M. Chhowalla, M. H. Gharahcheshmeh, K. K. Gleason, Y. S. Choi, B. H. Hong, and Z. F. Liu, Chemical vapour deposition, Nat. Rev. Methods Primers **1**, 5 (2021).

[60] C. S. Rout, P. V. Shinde, A. Patra, and S. M. Jeong, Recent developments and future perspectives of molybdenum borides and MBenes, Adv. Sci. **11**, 2308178 (2024).

[61] X. X. Xi, A. V. Pogrebnyakov, S. Y. Xu, K. Chen, Y. Cui, E. C. Maertz, C. G. Zhuang, Q. Li, D. R. Lamborn, J. M. Redwing *et al.*, MgB_2 thin films by hybrid physical-chemical vapor deposition, Phys. C (Amsterdam, Neth.) **456**, 22 (2007).

[62] S. Han, L. Yu, Y. Liu, B. Zhao, C. Wang, X. Chen, Y. Zhang, R. Yu, and X. Liu, Clathrate-like alkali and alkaline-earth metal borides: A new family of superconductors with superior hardness, Adv. Funct. Mater. **33**, 2213377 (2023).

[63] H. Xie, H. Wang, F. Qin, W. Han, S. Wang, Y. Wang, F. Tian, and D. Duan, A fresh class of superconducting and hard pentaborides, Matter Radiat. Extremes **8**, 058404 (2023).

[64] Z. Yuan, L. Hao, K. Luo, M. Xiong, C. Shao, F. Ling, and D. Yu, Structural stability, electronic structure, and superconductivity of cubic sodium hexaboride NaB_6 from first-principle calculations, Chem. Phys. Lett. **722**, 80 (2019).

[65] P. Zhang, Y. Tian, Y. Yang, H. Liu, and G. Liu, Stable Rb-B compounds under high pressure, Phys. Rev. Res. **5**, 013130 (2023).

[66] S. Chen, H. Xie, D. Xu, J. J. Chen, B. H. Cao, M. Liang, Y. B. Sun, X. Q. Gai, X. W. Wang, M. X. Yang, M. R. Zhang, D. F. Duan, D. Li, and F. B. Tian, Superconductivity of cubic MB_6 (M = Na, K, Rb, Cs), J. Chem. Phys. **160**, 044702 (2024).

[67] L. Wu, B. Wan, H. Liu, H. Gou, Y. Yao, Z. Li, J. Zhang, F. Gao, and H. Mao, Coexistence of superconductivity and superhardness in beryllium hexaboride driven by inherent multicenter bonding, J. Phys. Chem. Lett. **7**, 4898 (2016).

[68] H. J. Choi, S. G. Louie, and M. L. Cohen, Prediction of superconducting properties of CaB_2 using anisotropic Eliashberg theory, Phys. Rev. B **80**, 064503 (2009).

[69] L. Zhu, G. M. Borstad, R. E. Cohen, and T. A. Strobel, Pressure-induced polymorphism in SrB_6 and deformation mechanisms of novel covalent networks, Phys. Rev. B **100**, 214102 (2019).

[70] X. Yang, W. Zhao, L. Ma, W. Lu, X. Zhong, Y. Xie, H. Liu, and Y. Ma, Prediction of fully metallic σ-bonded boron framework induced high superconductivity above 100 K in thermodynamically stable Sr_2B_5 at 40 GPa, arXiv:2310.13945.

[71] L. Ma, X. Yang, G. Liu, H. Liu, G. Yang, H. Wang, J. Cai, M. Zhou, and H. Wang, Design and synthesis of clathrate LaB_8 with superconductivity, Phys. Rev. B **104**, 174112 (2021).

[72] Y. Liang, M. Xu, S. Lin, X. Yuan, Z. Qu, J. Hao, and Y. Li, Pressure-induced boron clathrates with ambient-pressure superconductivity, J. Mater. Chem. C **9**, 13782 (2021).

[73] V. A. Gasparov, N. S. Sidorov, I. I. Zver, and M. P. Kulakov, Electron transport in diborides: Observation of superconductivity in ZrB_2, J. Exp. Theor. Phys. Lett. **73**, 532 (2001).

[74] Y. Wang, J.-H. Tang, H.-R. Xu, G. Zhou, G. Ouyang, H.-X. Deng, R. D, and K. Yang, Nontrivial d-electrons driven superconductivity of transition metal diborides, New J. Phys. **26**, 063028 (2024).

[75] J. Meng, P. Zheng, Y. Peng, R. Liu, Y. Yang, and Z. Yin, Structure searches and superconductor discovery in XB_2 (X = Sc, Ti, V, Cr, and Tc), RSC Adv. **14**, 10507 (2024).

[76] Z. Qu, F. Han, T. Yu, M. Xu, Y. Li, and G. Yang, Boron kagome-layer induced intrinsic superconductivity in a MnB_3 monolayer with a high critical temperature, Phys. Rev. B **102**, 075431 (2020).

[77] X. Yuan, M. Xu, C. Huang, Y. Liang, S. Lin, J. Hao, and Y. Li, Pressure-stabilized MnB_6 that exhibits high-temperature ferromagnetism and high ductility at ambient pressure, J. Mater. Chem. C **10**, 4365 (2022).

[78] Y. Liang, M. Xu, Z. Qu, S. Lin, J. Hao, and Y. Li, A cage boron allotrope with high superconductivity at ambient pressure, J. Mater. Chem. C **9**, 8258 (2021).

[79] Y. Zhang, M. Xu, J. Hao, and Y. Li, Unveiling the influence of the boron clathrate lattice on superconductivity in a ternary Mg-La-B system, J. Mater. Chem. C **12**, 10678 (2024).

[80] S. Chen, Z. Wu, Z. Zhang, S. Wu, K.-M. Ho, V. Antropov, and Y. Sun, High-throughput screening for boride superconductors, Inorg. Chem. **63**, 8654 (2024).

[81] S. Aydin and M. Şimşek, A superconducting battery material: Lithium gold boride ($LiAu_3B$), Solid State Commun. **272**, 8 (2018).

[82] A. N. Kolmogorov, M. Calandra, and S. Curtarolo, Thermodynamic stabilities of ternary metal borides: An *ab initio* guide for synthesizing layered superconductors, Phys. Rev. B **78**, 094520 (2008).

[83] C. Zhou, H. Yu, Z. Zhang, Z. Yu, J. Zhu, K. Bao, and T. Cui, First-principles study on pressure-induced superconductivity and structural design on transition metal diborides, J. Chem. Phys. **161**, 084712 (2024).

[84] Z. Xiang, Y. Zhang, Q. Lu, Q. Li, Y. Li, T. Huang, Y. Zhu, Y. Ye, J. Sun, and H. Wen, Superconductivity up to 14.2 K in MnB_4 under pressure, Adv. Mater. **37**, 2416882 (2025).

[85] R. N. Shelton, Superconductivity and crystal structure of a new class of ternary platinum borides, J. Less Common Met. **62**, 191 (1978).

[86] E. V. Sampathkumaran and I. Das, Magnetic behavior of $CeIr_2B_2$, Phys. Rev. B **51**, 8628 (1995).

[87] J. M. Vandenberg, B. T. Matthias, E. Corenzwit, and H. Barz, Superconductivity of some binary and ternary transition-metal borides, Mater. Res. Bull. **10**, 889 (1975).

[88] F. Parvin and S. H. Naqib, Elastic, thermodynamic, electronic, and optical properties of recently discovered superconducting transition metal boride NbRuB: An *ab-initio* investigation, Chin. Phys. B **26**, 106201 (2017).

[89] Q. Zheng, W. Schnelle, Y. Prots, M. Bobnar, U. Burkhardt, A. Leithe-Jasper, and R. Gumeniuk, $AlPd_{15}B_7$: A new superconducting cage-compound with an anti-$Yb_3Rh_4Sn_{13}$-type of structure, Dalton Trans. **45**, 3943 (2016).

[90] H. Niimura, K. Kawashima, K. Inoue, M. Yoshikawa, and J. Akimitsu, Superconductivity in the ternary boride Cr_2Re_3B with the β-Mn-type structure, J. Phys. Soc. Jpn. **83**, 044702 (2014).

[91] B. Andrzejewski, Superconductivity in the Mo_2Re_3B compound, Cryogenics **48**, 478 (2008).

[92] K. Kawashima, A. Kawano, T. Muranaka, and J. Akimitsu, Superconductivity in intermetallic $W_7Re_{13}X$ (X = B and C) compounds, J. Phys. Soc. Jpn. **74**, 700 (2005).

[93] K. Kawashima, T. Muranaka, and J. Akimitsu, Superconductivity in intermetallic compound $Mo_7Re_{13}X$ (X = B, C), Sci. Technol. Adv. Mater. **7**, 9, 9 (2006).

[94] J. Lim, A. C. Hire, Y. Quan, J. S. Kim, S. R. Xie, S. Sinha, R. S. Kumar, D. Popov, C. Park, R. J. Hemley *et al.*, Creating superconductivity in WB_2 through pressure-induced metastable planar defects, Nat. Commun. **13**, 7901 (2022).

[95] G. Akopov, W. H. Mak, D. Koumoulis, H. Yin, B. Owens-Baird, M. T. Yeung, M. H. Muni, S. Lee, I. Roh, Z. C. Sobell *et al.*, Synthesis and characterization of single-phase metal dodecaboride solid solutions: $Zr_{1-x}Y_xB_{12}$ and $Zr_{1-x}U_xB_{12}$, J. Am. Chem. Soc. **141**, 9047 (2019).

[96] C. A. Nunes, D. Kaczorowski, P. Rogl, M. R. Baldissera, P. A. Suzuki, G. C. Coelho, A. Grytsiv, G. André, F. Boureé, and S. Okada, The NbB_2-phase revisited: Homogeneity range, defect structure, superconductivity, Acta Mater. **53**, 3679 (2005).

[97] Y. Singh, A. Niazi, M. D. Vannette, R. Prozorov, and D. C. Johnston, Superconducting and normal-state properties of the layered boride OsB_2, Phys. Rev. B **76**, 214510 (2007).

[98] K. Togano, P. Badica, Y. Nakamori, S. Orimo, H. Takeya, and K. Hirata, Superconductivity in the metal rich Li-Pd-B ternary boride, Phys. Rev. Lett. **93**, 247004 (2004).

[99] S. Bağcı, H. M. Tütüncü, H. Y. Uzunok, and G. P. Srivastava, *Ab initio* investigation of phonon-mediated superconductivity in the ternary borides Mo_5XB_2 (X = P, Si, Ge): Comparison with W_5SiB_2, Phys. Rev. B **109**, 144524 (2024).

[100] R. Wang, F. Zheng, Z. Zhang, S. Wu, H. Dong, C.-Z. Wang, V. Antropov, Y. Sun, and K.-M. Ho, Anticorrelation between electron-phonon coupling strength and stability of ternary metal diborides, Phys. Rev. B **111**, 014104 (2025).

[101] G. Bhaskar, V. Gvozdetskyi, M. Batuk, K. M. Wiaderek, Y. Sun, R. H. Wang, C. Zhang, S. L. Carnahan, X. Wu, R. A. Ribeiro *et al.*, Topochemical deintercalation of Li from layered LiNiB: Toward 2D MBene, J. Am. Chem. Soc. **143**, 4213 (2021).

[102] A. Bikowski, S. Siol, J. Gu, A. Holder, J. S. Mangum, B. Gorman, W. Tumas, S. Lany, and A. Zakutayev, Design of metastable tin titanium nitride semiconductor alloys, Chem. Mater. **29**, 6511 (2017).

[103] E. Arca, S. Lany, J. D. Perkins, C. Bartel, J. Mangum, W. H. Sun, A. Holder, G. Ceder, B. Gorman, G. Teeter *et al.*, Redox-mediated stabilization in zinc molybdenum nitrides, J. Am. Chem. Soc. **140**, 4293 (2018).

[104] R. Dronskowski and P. E. Bloechl, Crystal orbital Hamilton populations (COHP): Energy-resolved visualization of chemical bonding in solids based on density-functional calculations, J. Phys. Chem. **97**, 8617 (1993).

[105] S. Maintz, V. L. Deringer, A. L. Tchougreff, and R. Dronskowski, LOBSTER: A tool to extract chemical bonding from plane-wave based DFT, J. Comput. Chem. **37**, 1030 (2016).

[106] J. Hou, X.-J. Weng, A. R. Oganov, X. Shao, G. Gao, X. Dong, H.-T. Wang, Y. Tian, and X.-F. Zhou, Helium-nitrogen mixtures at high pressure, Phys. Rev. B **103**, L060102 (2021).

[107] E. Sanville, S. D. Kenny, R. Smith, and G. Henkelman, Improved grid-based algorithm for bader charge allocation, J. Comput. Chem. **28**, 899 (2007).

[108] P. Zhang, H. Guan, H. Li, X. Zhong, R. J. Hemley, and H. Liu, High-temperature superconductivity in quinary clathrate hydrides under pressure, Phys. Rev. B **112**, 054516 (2025).

[109] G. Kresse and J. Hafner, *Ab initio* molecular dynamics for open-shell transition metals, Phys. Rev. B **48**, 13115 (1993).

[110] G. Kresse, and J Furthmüller, Efficiency of *ab-initio* total energy calculations for metals and semiconductors using a plane-wave basis set, Comput. Mater. Sci. **6**, 15 (1996).

[111] P. E. Blöchl, Projector augmented-wave method, Phys. Rev. B **50**, 17953 (1994).

[112] J. P. Perdew, K. Burke, and M. Ernzerhof, Generalized gradient approximation made simple, Phys. Rev. Lett. **77**, 3865 (1996).

[113] P. Giannozzi, S. Baroni, N. Bonini, M. Calandra, R. Car, C. Cavazzoni, D. Ceresoli, G. L. Chiarotti, M. Cococcioni, I. Dabo *et al.*, quantum espresso: A modular and open-source software project for quantum simulations of materials, J. Phys.: Condens. Matter **21**, 395502 (2009).

[114] M. Schlipf and F. Gygi, Optimization algorithm for the generation of ONCV pseudopotentials, Comput. Phys. Commun. **196**, 36 (2015).

[115] F. Giustino, M. L. Cohen, and S. G. Louie, Electron-phonon interaction using Wannier functions, Phys. Rev. B **76**, 165108 (2007).

[116] S. Poncé, E. R. Margine, C. Verdi, and F. Giustino, EPW: Electron-phonon coupling, transport and superconducting properties using maximally localized Wannier functions, Comput. Phys. Commun. **209**, 116 (2016).